Journal of Hydrology 610 (2022) 127850

Contents lists available at ScienceDirect

Journal of Hydrology

journal homepage: www.elsevier.com/locate/jhydrol

Research papers

Response of surface evaporation and subsurface leakage to precipitation for simulated epikarst with different rock–soil structures

Jia Chen [a,b], Weijun Luo [a,c,d,*], Guangneng Zeng [e,*], Yanwei Wang [a,d], Yina Lyu [a,d], Xianli Cai [a,d], Lin Zhang [a,d], Anyun Cheng [a,c,d], Xinbao Zhang [f], Shijie Wang [a,d]

[a] State Key Laboratory of Environmental Geochemistry, Institute of Geochemistry, Chinese Academy of Sciences, Guiyang 550081, China
[b] University of Chinese Academy of Sciences, Beijing 100049, China
[c] College Rural Revitalization Research Center of Guizhou, Anshun 561000, China
[d] Puding Karst Ecosystem Research Station, Chinese Academy of Sciences, Puding 562100, China
[e] College of Eco-Environmental Engineering, Guizhou Minzu University, Guiyang 550025, China
[f] Institute of Mountain Hazards and Environment, Chinese Academy of Sciences, Chengdu 610041, China

ARTICLE INFO

This manuscript was handled by Huaming Guo, Editor-in-Chief

Keywords:
Rock–soil structure
Evaporation
Leakage
Rainfall intensity
Lysimeter

ABSTRACT

Karst water is an extremely important resource and can respond to precipitation events quickly due to the high rock exposure rate, shallow and uneven soil layers, and various crack sizes. The impacts of this special rock–soil structure type on hydrological processes are difficult to quantify, mainly because the karst subsurface structure is very complex. In this study, lysimeters representing four rock–soil structures with two rock exposure rates (50% and 80%) and two soil thicknesses (5 cm and 20 cm) were constructed at the Puding Karst Ecosystem Research Station, Chinese Academy of Sciences. The following results were obtained by observing the evaporation and leakage from September 2019 to August 2020. 1) Over a year, the evaporation of the 80% rock exposure lysimeter was approximately 8% less than that of the 50% rock exposure lysimeter, while the two lysimeters with different soil thicknesses had only a 2% difference in evaporation. 2) The surface evaporation of different rock exposure rates varies greatly after different rainfall intensities. However, there was no significant change in surface evaporation between different soil thicknesses after rainfall of different intensities. 3) Generally, with the increase in the rock exposure rate, the infiltration coefficient nonlinearly increased. The leakage coefficients for cracks of different sizes and different soil thicknesses were approximately 0.67 and 0.57, respectively. 4) The amount of leakage and the time to reach the peak flow varied greatly among different rock–soil structures and were also affected by the antecedent rainfall. Thus, rock exposure has a great impact on surface evaporation after rainfall, and the influence of cracks on subsurface hydrological processes was greater than that of soil thickness. These findings can provide a scientific reference for water use and management practices in karst areas.

1. Introduction

Karst is widely distributed in the world, accounting for approximately 12% of the land area (Hartmann et al., 2014). Approximately 20–25% of the world's water resources mainly depend on karst groundwater (Stevanovic, 2018), providing water for nearly 25% of the world's population (Hartmann et al., 2014; Andreo, 2012). Due to the extremely complex surface cover conditions of karst, the spatial differences in crack size, rock exposure rate and soil thickness are obvious (Fig. 1), and there are great differences in surface and subsurface hydrological processes in epikarst zones with different rock–soil structures (Zhang et al., 2018; Wang et al., 2015; Fu et al., 2007; Ford and Williams, 2007). In karst areas, when rain falls on the ground, it quickly flows underground and collects in the discharge area, resulting in a relative shortage of available water for surface vegetation (Luo et al., 2014), as well as droughts and floods occurring frequently in laeuna (Nie et al., 2012). The study of surface water evaporation and groundwater hydrological processes can reveal the regional water dynamics and transformation law, guide drought and waterlogging prevention measures and direct the utilization and management of karst water

* Corresponding authors at: State Key Laboratory of Environmental Geochemistry, Institute of Geochemistry, Chinese Academy of Sciences, Guiyang 550081, China (W. Luo).
E-mail addresses: luoweijun@vip.gyig.ac.cn (W. Luo), augustinezeng@gzmu.edu.cn (G. Zeng).

https://doi.org/10.1016/j.jhydrol.2022.127850
Received 4 November 2021; Received in revised form 14 April 2022; Accepted 16 April 2022
Available online 21 April 2022

resources.

Generally, the change in rock–soil structure is considered to be an important factor causing the spatial heterogeneity of soil moisture (Shen et al., 2019), and such nonsoil components can be included in the soil profile to form a hydrological model of the soil–plant-atmosphere continuum (Ford and Williams, 2007). At the same time, the geological structure and geomorphology of the surface can affect the surface hydrological processes (Seneviratne et al., 2010; Hamilton and Ford, 2002). Previous studies have suggested that rock fragments resting on the soil surface or partly incorporated in the topsoil affect water leakage, rock flow, surface runoff and evaporation (Poesen and Lavee, 1994). An increase in the rock exposure rate can reduce the soil water demand per unit space, reduce surface evaporation, and increase water leakage at the rock–soil interface (Zhao et al., 2020). In addition, simulation calculations have shown that the catchment exposure rate increased and decreased by 20% and that the evaporation decreased and increased by 13.1% and 11.2%, respectively (Zhang et al., 2013b). Although the above-mentioned studies have shown that the rock exposure rate affects the surface evaporation process, there are many factors affecting evaporation in a basin, and it is difficult to accurately measure evaporation, so it is difficult to explore the effects of different rock exposure rates and soil thickness on surface evaporation alone in the natural environment. Therefore, more quantitative information to clarify the impact of rock–soil structure on surface hydrological processes can make an effective contribution to further understanding the surface evaporation process of karst environment (Ferreira et al., 2021; Zhao et al., 2018; Poesen and Lavee, 1994).

At the same time, highly exposed rock, cracks and thin soil layers, all of which may have a significant impact on the process of infiltration and groundwater recharge (Sohrt et al., 2014), result in rapid water infiltration into the deep subsurface (Goldscheider et al., 2020; Hao et al., 2012; Butscher and Huggenberger, 2009). One study observed a positive correlation between the stone coverage area and infiltration coefficient of soil (Wilcox et al., 1988). Moreover, both soil thickness and rock porosity lead to the complexity of groundwater movement features (Bakalowicz, 2005; Jones et al., 2000). This also shows that the rock–soil structure has a great impact on the underground hydrological processes. In addition, rainfall intensity is also another important factor. Other studies divided runoff into fast flow and diffuse flow by using a principal regression curve and demonstrated the relationship between rainfall intensity and flow velocity, with 5 times faster velocities for quick recharge flow than diffuse flow (Poulain et al., 2018), and stream water was generated when rainfall intensity reached 10–15 mm/h in a certain basin (Wang et al., 2020a). The above studies have pointed out that cracks, soil thickness and rainfall intensity affect the subsurface hydrological processes. However, due to the change in meteorological conditions and the difference in geological conditions, the hydrological processes of the surface and subsurface areas of karst change every year (Massei et al., 2007), and there are many factors affecting the hydrological processes of the basin. Therefore, how to quantify the influence of rock–soil structure on the leakage coefficient and dynamic hydrological processes under different rainfall characteristics still needs to be studied in depth (Wang et al., 2020a; Sohrt et al., 2014; Poesen and Lavee, 1994), It provides useful information for acknowledge of karst hydrological behaviours.

Some previous studies have investigated the differences in evapotranspiration among different land use types by establishing a simulation test site (Hu et al., 2018). The dynamic response of groundwater to hydrological factors has also been studied by simulating a karst aquifer system (Ding et al., 2020). However, the different structures of rock and soil can form various microenvironments on the surface, and the subsurface structure is complex, these factors makes the hydrological processes more complicated, making it difficult to research its impact on the surface and groundwater hydrological processes in a natural watershed. In view of the above ideas of simulation research, we established four lysimeters with different rock–soil structures according to the rock–soil ratio (1:1 and 1:4) and soil thicknesses (5 cm and 20 cm), and surface evaporation and subsurface leakage were monitored from September 2019 to August 2020. The present study aimed to quantitatively study (1) the influences of the rock–soil structure on surface evaporation and groundwater hydrological processes and (2) the surface and subsurface hydrological responses of different rock-soil structures after different rainfall intensities.

2. Materials and methods

2.1. Study area

The lysimeters were located at the Puding Karst Ecosystem Research Station, Chinese Academy of Sciences (26°14′-26°15′ N, 105°42′-105°43′ E), in Puding County, Guizhou Province, Southwest China. There, the annual average temperature is 15.1 °C (33 °C to −5 °C), the annual average sunshine hours are 1,165 h, the annual average frost-free period is 301 days, the annual average humidity is 78%, and the multiyear average precipitation is 1,315 mm (1,769 mm to 758 mm), which is mainly concentrated in the rainy season (May to October), accounting for more than 80% of the total annual rainfall (Zhao et al., 2010).

2.2. Lysimeter

There were four lysimeters for simulating the water cycle in the epikarst zone with different rock–soil structures (Fig. 2). Each lysimeter is 50 cm apart and is located in the outdoor natural environment. The tanks were made of welded carbon steel with a thickness of 8 mm and a volume of 2 m × 2 m × 2 m. To maintain stability, the tank was placed on the weighing platform and supported by the weighing sensor, which was placed on the foundation bed, and the accuracy of the weighing

Fig. 1. High exposure rate and developmental crack (left, limestone); thin and even surface soil (right, dolomite).

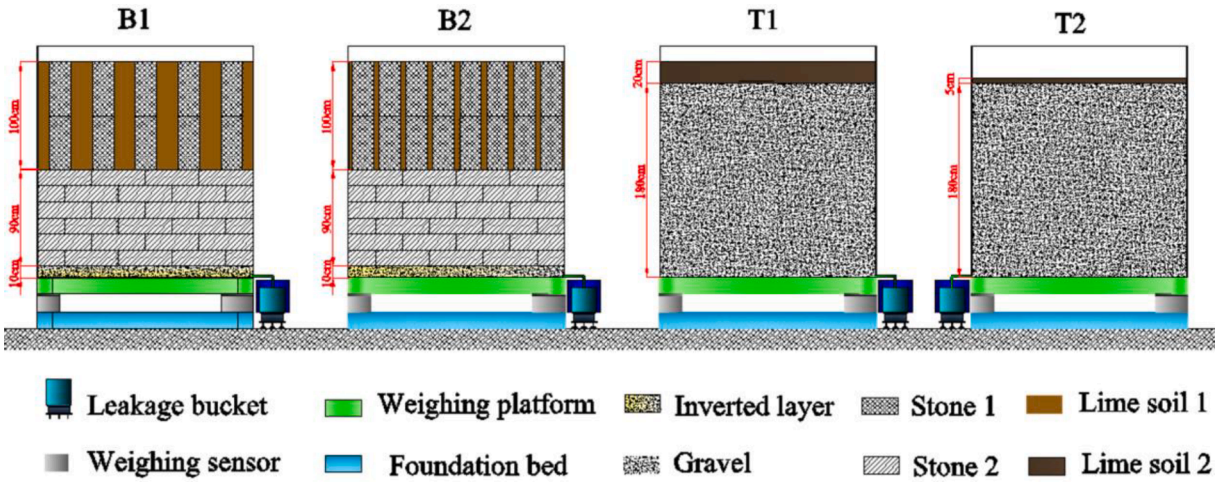

Fig. 2. Schematic diagram of different rock–soil structures.

system was 400 g. There was a round outlet with a diameter of 15 mm at the bottom of each tank, which was kept permanently open. The leakage water directly flowed into the leakage bucket, which was directly weighed by the weighing sensor. The volume of the leakage bucket was 10 L, and an automatic electronic valve was installed at the bottom. When the total leakage was more than 3 kg, the leakage bucket drained automatically, and the accuracy of the leakage weighing system was 40 g.

It can be seen from the rock–soil structure in the left figure (Fig. 1) that the rock exposure rate is high and the crack size is different. To facilitate the calculation of the rock exposure rate and crack size, stones with regular shapes are used to fill the lysimeters in this study. Moreover, the soil thickness in the dolomite area is shallow (Fig. 1), and the exposure rate of the bedrock is low. The method of direct soil covering is adopted in this study. At the same time, on the basis of long-term field investigation and summarizing previous research (Wu et al., 2021), high rock exposure rates of 50% and 80% and soil thicknesses of 5 cm and 20 cm are selected for comparative research to explore the impact of rock–soil structures on surface evaporation and underground leakage. Previous studies have shown that the surface runoff yield in karst areas is

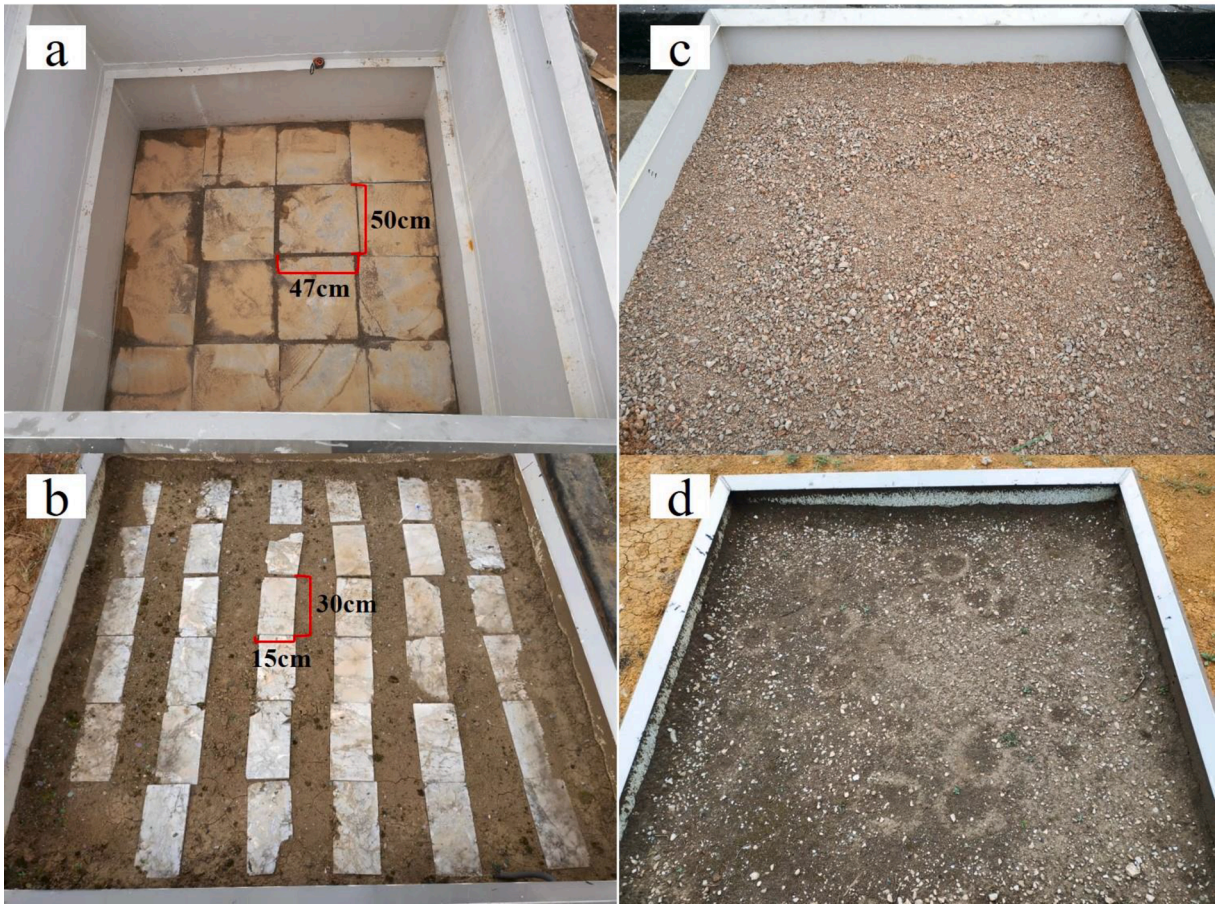

Fig. 3. Interior filling diagram of different rock–soil structures.

less than 5% (Peng and Wang, 2012; Chen et al., 2020). Therefore, the collection and observation of surface runoff are not considered in this study. The lysimeter of tank B1 was filled as follows: a layer of 10 cm thick limestone gravel (with particles approximately 0.5 cm in diameter) formed by an inverted layer was placed at the bottom of tank B1, regular stones 2 (15 cm × 50 cm × 47 cm) were placed to reach a height of 90 cm (Fig. 3a), and the gaps between the blocks were filled with rock powder to form the bedrock. The upper part was composed of regular stones 1 (50 cm × 30 cm × 15 cm) and lime soil, with a height of 100 cm, in which the soil comes from lime soil in cracks in the natural environment. Therefore, the surface rock exposure rate of B1 is 50%, and the width of the cracks is 15 cm (Fig. 3b). The bottom treatment of tank B2 was the same as that of tank B1, but the difference in the rock–soil structure was that the cracks included in the upper part were 5 cm wide, and the surface rock exposure rate was 80%. The bottom of tank T1 was filled with dolomite gravel that had passed through a 2 cm sieve, with a height of 180 cm and a porosity of 0.4 (Fig. 3c), and the topsoil collected from the lime soil on a dolomite mountain was laid on top to form a layer with a thickness of 20 cm (Fig. 3d). The difference between tank T2 and tank T1 was that the thickness of the topsoil in tank T2 was 5 cm. The soil physical properties and the rock chemical properties are shown in Table 1 and Table 2.

2.3. Data collection and calculation

The construction of the lysimeters was completed in May 2018, and the development of the weighing sensor system was completed in August. After one year, the data of a whole hydrological year, from September 2019 to August 2020, were used to capture the influences of rock–soil structure on hydrological processes. During this study period, there was no vegetation on the surface, and when any grass that grew was pulled out in time.

Evaporation (E), leakage (Q) and the aquifer infiltration coefficient (α) are important parameters for the evaluation of hydrological processes in this study.

Evaporation was calculated as follows:

$$E = P - Q - \Delta W \tag{1}$$

$$E = P - Q - (W_t - W_{t-1}) \tag{2}$$

The aquifer infiltration coefficient (α) was calculated as follows:

$$\alpha = Q/P \tag{3}$$

where P is precipitation in mm; Q is the leakage, which is directly measured by the leakage system and converted into the water level, in mm; and W_t and W_{t-1} are the total weight of the tank at t hour and t-1 h, respectively, and unit area depth, in mm. The unit of E is mm. Among them, Q and W are directly measured by the weighing system, and P is obtained by the rain gauge of the meteorological station. When there is rainfall, E can be calculated from the measured P and the changes in Q and △W. When there is no rainfall, E can be calculated from the difference between the change in △W and Q.

In addition, meteorological parameters, such as precipitation (P), air temperature (T), relative humidity (RH), net radiation (Rn) and wind speed (WS), were obtained directly from the weather station (approximately 100 m from the lysimeters) at a frequency of once an hour.

Table 1
Physical properties of soil from the lysimeter.

Physical properties	bulk density ($g.cm^{-3}$)	Clay (<0.002 mm)	Silt (0.002–0.02 mm)	Sand (0.02–2 mm)
Lime Soil 1	1.3	11.8	65.4	22.8
Lime Soil 2	1.0	6.0	48.4	45.6

2.4. Statistical analysis

Statistical analysis was conducted using SPSS software (ver. 19.0, SPSS Inc. Chicago, IL, USA). Pearson correlation analysis was used to explore the correlation between evaporation and meteorological factors of four lysimeters in rainy season and dry season, the significant differences were evaluated at the p less than 0.05, and the very significant differences were evaluated at the p less than 0.01. The relationship between rainfall and leakage was analyzed by linear regression. Graphic plotting of curves was conducted with Origin 9.2 (Origin Lab, Northampton, MA, USA). The schematic diagram of different rock–soil structures was drawn with the AutoCAD 2007 (Autodesk, California, USA) software.

3. Results

3.1. Meteorological factors

The daily dynamic characteristics of the evaporation and meteorological factors (P, T, RH, WS and Rn) of the four rock–soil structures are presented in Fig. 4. Precipitation has obvious seasonal variation and is mainly concentrated from May to October, accounting for 89% of the annual precipitation. The temperature shows a trend of low in the dry season (mean 11 °C) and high in the rainy season (mean 21.8 °C), and the maximum and minimum daily average temperatures are 28.7 °C and 3 °C, respectively, with an annual average temperature of 16.4 °C. The fluctuation range of relative humidity is 45% − 100%, and the annual average relative humidity is 80%. The average wind speed from January to April is 1.9 m/s, and the average wind speed in other months is 1.4 m/s. The difference in Rn between the dry season and rainy season is large, and the average net radiation is 3.7 MJ/m^2 in the dry season and 8.06 MJ/m^2 in the rainy season. Due to the influence of uncontrollable factors (power failure, instrument failure, etc.), the weighing system could not weigh the system, resulting in the loss of data for several days in May, June and July, but it does not affect the analysis of the pattern of change in annual evaporation. The surface evaporation of the four rock–soil structures is generally low in the dry season, following the seasonal variation trends of rainfall, temperature and net radiation.

3.2. Evaporation process

3.2.1. Changes in monthly evaporation

The variations in monthly evaporation with rainfall in each of the four tanks are shown in Fig. 5. The surface evaporations of different rock–soil structures are greatly affected by rainfall and have a good corresponding relationship with the seasonal variation in rainfall. Throughout the year, evaporation in the rainy season accounts for approximately 70% of the total evaporation. The annual evaporation of B1, B2, T1 and T2 are 390 mm, 361 mm, 498 mm and 486 mm, respectively. The evaporation in B1 is only 30 mm more than that in B2. The difference between T1 and T2 is very small. The evaporation without rock exposure is higher than that with rock exposure, which is approximately 100–120 $mm{\cdot}year^{-1}$. However, in the rainy season, the evaporation without rock exposure is significantly higher than that with rock exposure, up to approximately 10–27 $mm{\cdot}month^{-1}$. In the dry season, the surface evaporation results of the four simulation fields are similar, and the highest is only 5 $mm{\cdot}month^{-1}$. Therefore, the influence of the rock exposure rate on surface evaporation is mainly reflected in the rainy season.

It can be seen from Fig. 5 that the surface evaporation increased in January because the rainfall increased significantly in January, resulting in an increase in surface evaporable water. However, the evaporation in October is higher than that in September, which is related to the rainfall distribution. Combined with the daily rainfall in Fig. 4, it can be seen that the rainfall in September is concentrated in the first 10 days, with strong surface evaporation in the early stage and weak surface

Table 2
Chemical compositions of rock from the lysimeter.

Chemical composition	SiO_2	Al_2O_3	Fe_2O_3	MgO	CaO	Na_2O	K_2O	MnO	P_2O_5	TiO_2	SO_3	LOI[a]	SUM
Stone (%)	0.40	0.25	0.39	20.67	31.59	0.02	0.08	0.016	0.019	0.020	0.060	46.24	99.74
Gravel (%)	0.92	0.35	0.21	20.91	30.98	0.02	0.10	0.016	0.024	0.015	0.071	46.06	99.66

LOI [a] is an abbreviation for loss on ignition at approximately 1000 °C.

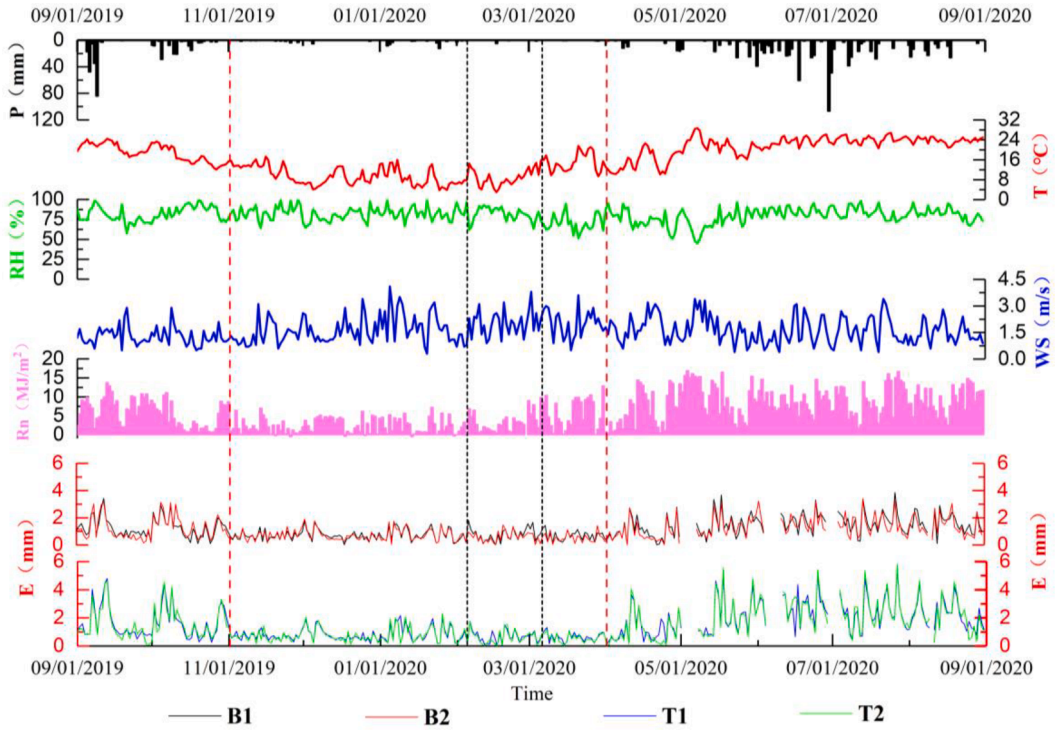

Fig. 4. Daily average values of precipitation (P), temperature (T), relative humidity (RH), wind speed (WS), net radiation (Rn) and evaporation (E) at the four lysimeters.

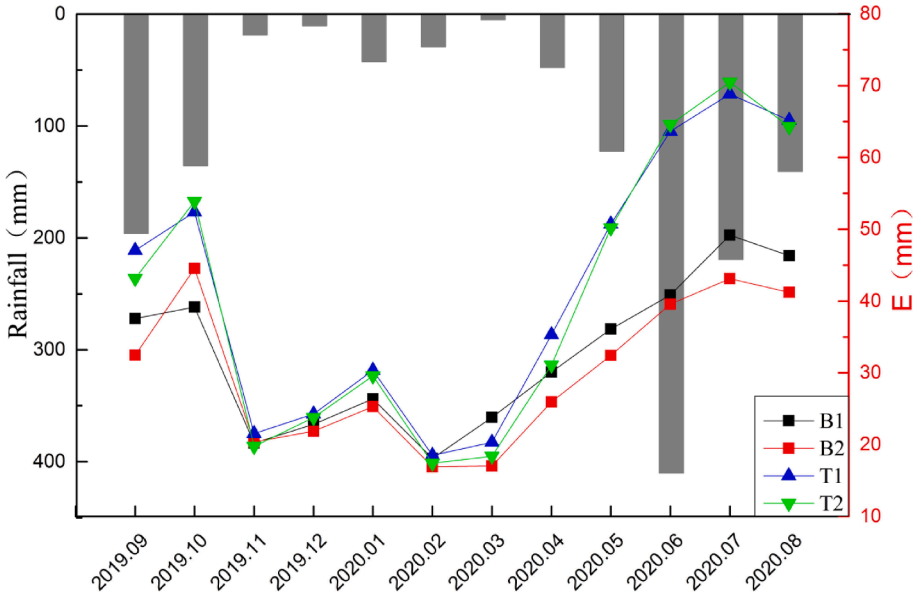

Fig. 5. Changes in monthly rainfall and evaporation.

evaporation in the later stage. The total amount of rainfall in October is small, but the distribution is discrete, so the surface evaporation in the whole month will be higher. The turning point of evaporation in June, July and August is also related to rainfall and rainfall distribution. At the same time, the missing 6-day data in June have a certain error in the statistics of monthly evaporation. Therefore, the total amount and

distribution of rainfall can also affect surface evaporation. However, a few of vegetation on the surface of the lysimeter may not be removed in time during the study period, which may affect the evapotranspiration.

3.2.2. Evaporation after different rainfall intensities

The variation in surface evaporation after different rainfall intensities is presented in Fig. 6. There are significant differences in evaporation between B1 and B2 during heavy rainfall, light rainfall and no rainfall periods. After heavy rainfall, which is a total rainfall in 12 h of more than 15 mm, the surface evaporation of B2 is significantly higher than that of B1, with an average surface evaporation rate of 0.06 mm/h and a maximum surface evaporation rate of 0.3 mm/h. However, after light rainfall, which is a total rainfall in 12 h of less than 15 mm, the surface evaporation of B1 and B2 increases or decreases in a fluctuating manner, but there is little difference overall. Nevertheless, in the no rainfall periods, the surface evaporation of B1 is initially slightly higher than that of B2, with an average value of 0.07 mm/h. However, after different rainfall intensity events, the surface evaporation of T1 and T2 shows the same change rule and no significant difference and thus does not change with the change in rainfall intensity. Therefore, the surface evaporation after different rainfall intensities is significantly affected by the rock exposure rate but not by the soil thickness (Fig. 6). This may be related to the water stored on the bare rock surface, and the water evaporation on the rock surface is also part of the surface evaporation. The silt and sand contents in soils with different thicknesses are 48.4% and 45.6%, respectively. The water holding capacity of soil is poor, and the surface area affected by evaporation is the same, so there is no significant difference in evaporation.

3.3. Leakage process

3.3.1. The leakage and infiltration coefficient

Table 3 shows that the total leakages of the four lysimeters during the observation period are between 790 mm and 917 mm, and 96% of the leakage is concentrated in the rainy season. Among them, the total leakage of B1 is only 10 mm higher than that of B2, and the difference in the infiltration coefficient is approximately 1%. However, due to the difference in rainfall in each month, the leakage of B1 and B2 is obviously different, especially in January and April. The leakage of B2 is significantly higher than that of B1 because rainwater mainly infiltrates along the rock–soil interface, and the area of the rock–soil interface of B2 is greater than that of B1. At the same time, because some water can be retained in the soil and pores of different rock–soil structures, which will lead to leakage lag, resulting in the sum of evaporation and leakage being higher than rainfall. The total amount of leakage in T1 is only 17 mm lower than that in T2, and the difference in the infiltration coefficient is approximately 2%, but the difference between the two is small relative to the difference in rainfall. However, there is a large difference in the amount of leakage between structures with cracks (B1, B2) and without cracks (T1, T2), which is approximately 100 mm, and the difference in the infiltration coefficient is up to 10%. Therefore, in the case of the same rainfall, the leakage is affected by the rock–soil structure and thus varies among the lysimeters, indicating that the hydrological processes are affected by the rock–soil structure.

3.3.2. Leakage after different rainfall intensities

The dynamic characteristics of leakage at each lysimeter are shown in Fig. 7. The time series analysis of runoff during rainfall shows that when the continuous rainfall is more than 10 mm/h, the leakage of the epikarst zone increases significantly. There were two observation periods of note (September 6–10, 2019; June 15–25, 2020). In the first observation period, there were two continuous heavy rainfall events with total precipitations of 63.8 mm and 108.2 mm and maximum rainfall intensities of 15 mm/h and 14.8 mm/h, respectively. The peak times of the leakage in the structure with cracks (B1, B2) are significantly faster than those of the structure without cracks (T1, T2) in the period (Fig. 8). Additionally, the peak flows of the structure with cracks are higher. However, in the second observation period, there was one heavy rainfall event and three moderate rainfall events, with rainfalls of 13.8 mm and 60.4 mm and 23.6 mm and 20.4 mm, respectively, and the maximum rainfall intensities were 11.6 mm/h and 31.4 mm/h and 16.4 mm/h and 6.2 mm/h, respectively. At this stage, the time when the leakage of the four lysimeters reaches the peak value is quite different, but the peak flow of the lysimeters with different crack sizes (B1, B2) is also higher than that of the structures with different soil thicknesses (T1, T2). The reasons for the above differences among different rock–soil structures may be mainly affected by the total amount of rainfall, rainfall intensity and rainfall in the early stage. The two rainfall events in the first period are higher than the two rainfall events with the same maximum rainfall intensity in the second period, and their peak leakage is greater. When the rainfall intensity increases, the rainwater will rapidly infiltrate through the preferential flow, fissure flow and soil saturated infiltration formed at the rock–soil interface. Therefore, for the two rainfall events with the same total rainfall in the two periods, the greater the rainfall intensity is, the greater the leakage and the faster the time to reach the peak. In the second period, the maximum rainfall intensity of 16.4 mm/h is smaller than that of 6.2 mm/h, which is related to whether there is rainfall in the early stage. However, under the same rainfall conditions, the leakage process between different rock–soil structures were also different, which also shows that the rainfall intensity and rock–soil structure have a great impact on the hydrological process.

4. Discussion

4.1. Effect of environmental factors on evaporation

Many previous studies have analysed the effects of environmental factors on evapotranspiration. For example, in the temperate climate of Oklahoma, USA, relative humidity and temperature have the greatest impacts on evapotranspiration (Coleman and decoursey, 1976). Under the arid and semiarid climate of cultivated land in Iran, the main controlling factor of evapotranspiration is solar radiation (Nouri et al., 2017). In the various geomorphic landscapes in the Yangtze River Basin, relative humidity has the greatest impact on evapotranspiration, followed by shortwave radiation, temperature and wind speed (Gong et al., 2006). In Australian woodlands, precipitation is a key factor affecting evapotranspiration (Zeppel et al., 2008). The spatial variation in surface evapotranspiration in China is mainly dominated by annual total net radiation, average annual precipitation and average temperature (Zheng et al., 2016). In karst areas, temperature, precipitation and photosynthetic effective radiation have a greater impact on evapotranspiration, while wind speed and relative humidity have less of an impact (Zhang et al., 2018). Through the Pearson correlation analysis (Table 4), this study shows that in the dry season, the net radiation shows a very significant positive correlation, while the relative humidity shows a very significant negative correlation. In the rainy season, except for the rock–soil structure with a rock exposure rate of 80%, other rock–soil structures have a very significant positive correlation with temperature, wind speed and net radiation. Generally, wind speed and relative humidity promote evaporation (Lenters et al., 2005). As rainwater directly supplies soil water, it affects surface evaporation. In the dry season, due to the lower rainfall, and the higher the relative humidity is, the smaller the surface evaporation. However, in the rainy season, the greater the rainfall is, the higher the temperature, wind speed and net radiation, resulting in a higher surface evaporation intensity. However, the rock–soil structure with an 80% rock exposure rate may be affected by many cracks, rapid rainwater and evaporation of rock moisture, resulting in a significant relationship between evaporation and wind speed and net radiation.

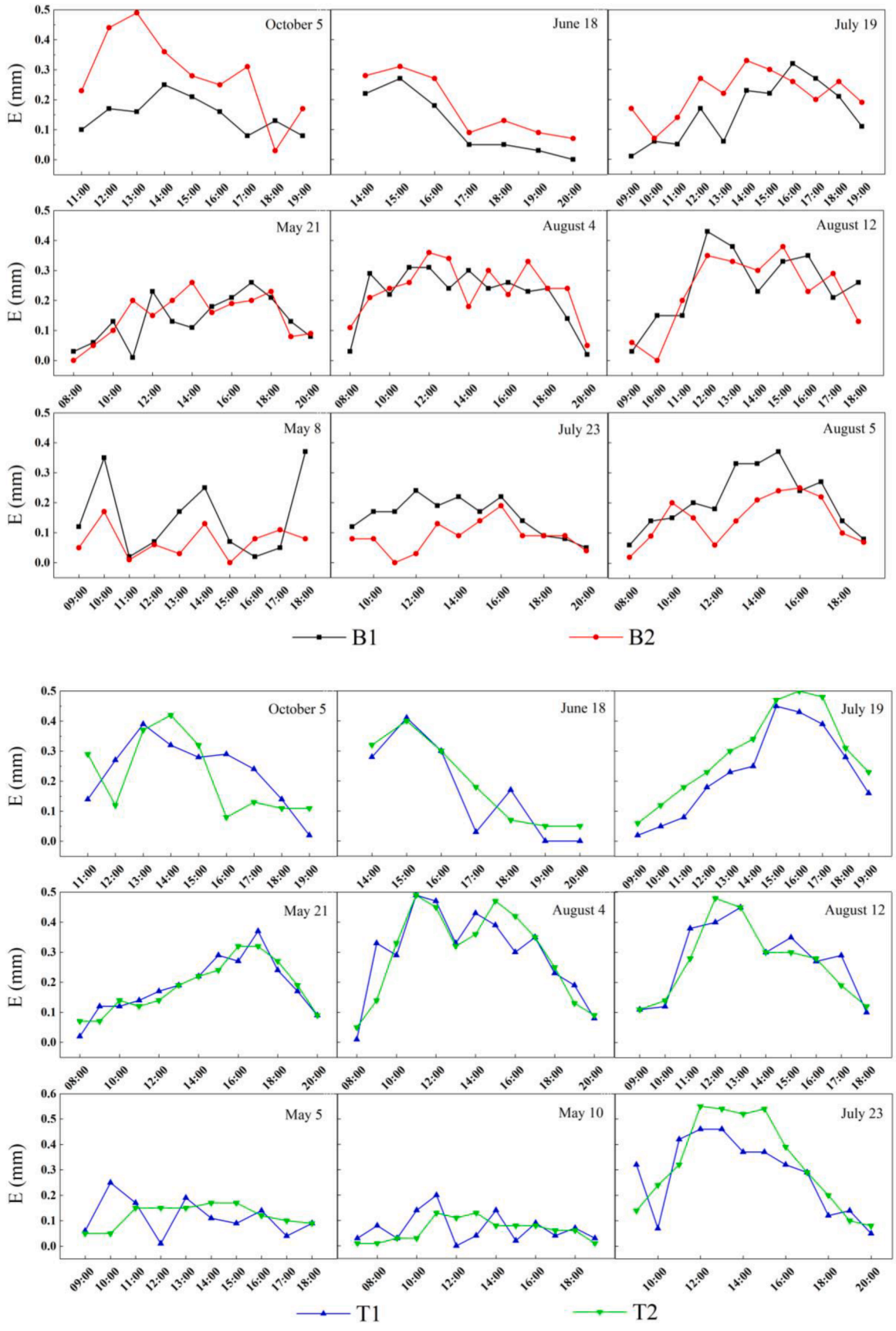

Fig. 6. According to the precipitation grade table of the ecosystem atmospheric environment observation standard, precipitation less than 14.9 mm in 12 h is moderate rain and light rain. Heavy rain and rainstorms occur when the precipitation over 12 h is more than 15 mm. In this study, the days of heavy rainfall are October 5 (28.8 mm), June 18 (60.6 mm), and July 19 (27.8 mm). The times of light rainfall were May 21 (7.4 mm), August 4 (6.4 mm), and August 12 (6.0 mm). The rest of the time corresponds to the no rainfall period.

Table 3
Dynamic variation in monthly precipitation and leakage.

Test site	Sep (mm)	Oct (mm)	Nov (mm)	Dec (mm)	Jan (mm)	Feb (mm)	Mar (mm)	Apr (mm)	May (mm)	Jun (mm)	Jul (mm)	Aug (mm)	Total (mm)	α (%)
P	195.8	135.4	18.6	10.4	42.4	29.0	5.0	47.6	122.4	410.2	219.2	140.4	1,376.4	
B1	160.5	81.4	5.8	0.5	5.9	8.3	2.7	4.9	56.2	337.7	147.0	106.3	917.2	0.67
B2	147.8	85.2	3.4	0.1	10.7	5.3	1.1	11.2	64.1	315.0	154.7	108.5	907.0	0.66
T1	145.2	64.3	9.4	2.3	1.4	3.7	5.2	3.1	31.4	298.2	138.6	87.5	790.2	0.57
T2	152.1	66.6	8.8	3.2	0.2	5.6	9.6	5.1	37.3	294.3	132.9	91.6	807.2	0.59

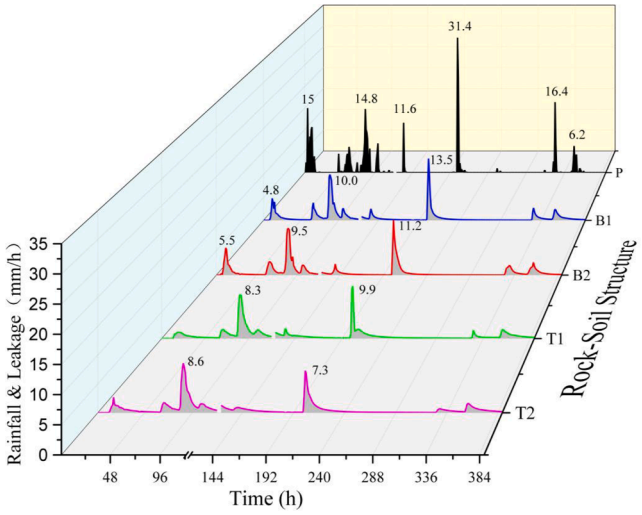

Fig. 7. The dynamic change characteristics of leakage at each lysimeter after different rainfall events. The time periods are from September 5, 20:00, 2019, to September 10, 20:00, 2019, at 1 to 121, and from June 14, 20:00, 2020, to June 25, 20:00, 2020, at 124 to 388.

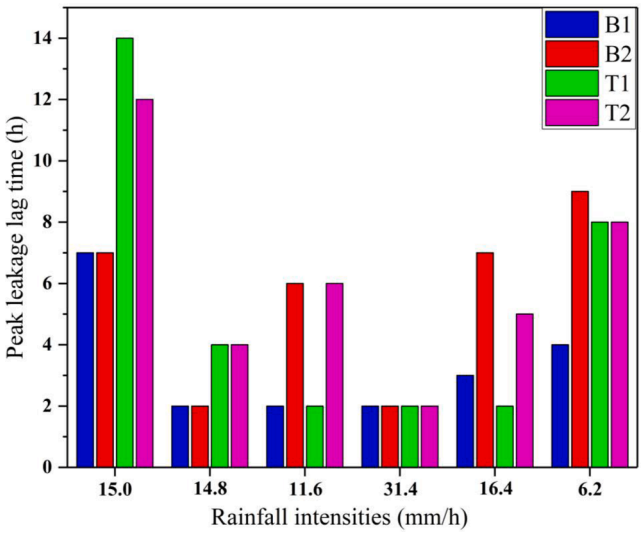

Fig. 8. The relationship between maximum rainfall intensity and peak leakage lag time.

4.2. Response of surface evaporation to rainfall events

In the same environment, because there are no plants in the bare land, surface evaporation is mainly affected by the surface environment. The lower the rock exposure is, the larger the soil surface area under evaporation, and the higher the evaporation. However, for the completely covered cases, the annual evaporation of T1 is only 12 mm

Table 4
Pearson correlation analysis of meteorological factors and evaporation for different rock–soil structures.

Lysimeter	Season	P	T	RH	WS	Rn
B1	Dry	−0.016	0.242**	−0.436**	0.120	0.566**
	Rainy	−0.101	0.362**	−0.135	0.250**	0.467**
B2	Dry	0.009	0.007	−0.263**	0.078	0.310**
	Rainy	0.104	0.133	0.100	0.153*	0.192*
T1	Dry	−0.011	0.138	−0.410**	0.140	0.448**
	Rainy	−0.089	0.334**	−0.088	0.241**	0.470**
T2	Dry	−0.018	0.112	−0.362**	0.054	0.467**
	Rainy	−0.053	0.298**	−0.050	0.232**	0.453**

** indicates a very significant difference at the confidence level of p less than 0.01.
* indicates a significant difference at the confidence level of p less than 0.05.

higher than that of T2, because of the water holding capacity of the soil, evaporation mainly occurs at the surface, and the thicker soil has a higher water supply capacity. A model has been used to calculate that soil evaporation decreases by 13.1% when the rock exposure rate of the basin increases by 20% and that the soil evaporation increases by 11.2% when the rock exposure rate of the basin decreases by 20% (Zhang et al., 2013b). Notably, precipitation has a significant promoting effect on evapotranspiration. The transpiration of plants increases significantly after rain (P greater than 20 mm·day^{-1}) (Zeppel et al., 2008), and the rocks on the surface of the soil affect rainfall interception and surface evaporation (Poesen and Lavee, 1994). We find that there is a significant difference in evaporation between the experimental sites with different rock exposure rates after different intensities of rainfall events, in contrast, there is little difference in evaporation between the simulated fields with different soil thicknesses. This may be because after a heavy rainfall event, the rock is sufficiently wet, part of the rainwater is stored as rock moisture (Rempea and Dietrich, 2018) or some rainwater from a depression on the rock surface, and the specific heat capacity of rock is lower than that of soil. These factors lead to the evaporation of the rock surface being stronger than that of the soil for a short time after the rainfall event. When the evaporation of the rock surface is dominant, the higher the exposure rate of the rock is, the greater the evaporation. However, after a light rainfall event, the difference in evaporation between the soil and rock surfaces is small. During a long period of no rainfall, evaporation is mainly from the soil, thus, evaporation is greater for a lower rock exposure rate. When there is no exposed rock, evaporation is only controlled by the soil, so after any rain, the difference in evaporation between the structures with different soil thicknesses has little difference. Therefore, the rock exposure rate significantly affects the surface evaporation after any intensity of rainfall, while the soil thickness has little effect on the surface evaporation.

4.3. Influence of the rock–soil structure on the infiltration coefficient

The infiltration coefficient of the epikarst zone is controlled by the rock–soil structure. However, the infiltration coefficient is different under different rainfall intensities. The initial water filling degree of the crack structure in the epikarst zone greatly affects the rainfall infiltration, thus affecting the storage capacity of the epikarst zone (Zou et al.,

2005). A previous study pointed out that the infiltration coefficient of a simulation field with a soil thickness of 50 cm is 0.57, while the infiltration coefficient of a simulation field with a rock exposure rate of 100% is 0.9 (Zeng et al., 2017). According to the results of this study (Table 3), the infiltration coefficient is less than 0.6 in the case of no exposed rock, more than 0.6 in the case with some exposed rock, and 0.9 in the case of 100% rock exposure (Zeng et al., 2017). With the increase in the rock exposure rate, the infiltration coefficient nonlinearly increases, which may be mainly related to surface evaporation. When there is no exposed rock, due to the interception and conservation of soil water, the surface evaporates a large amount of water, resulting in a small infiltration coefficient. When there are exposed rocks and cracks, part of the rainwater flows into the ground quickly, and the amount of surface water that evaporates is small, which leads to an increase in the infiltration coefficient. When the rock exposure rate is 100%, rainfall flows into the ground rapidly, the evaporation of rock moisture is the main part, and the evaporated water is about 10%. A possible explanation for this trend is that the increase in rock exposure gradually decreases the soil quantity and soil moisture storage capacity per unit of space and increases the water leakage at the soil–rock interface (Zhao et al., 2020). However, the relative change in the rock exposure rate and soil thickness has little influence on the infiltration coefficient. For example, when the soil thickness increases from 5 cm to 50 cm or the rock exposure rate increases from 50% to 80%, the difference in the infiltration coefficient is small. This may be related to the local rainfall characteristics, because approximately 90% of the precipitation is concentrated in the rainy season, the thin soil and the existence of cracks lead to the rapid infiltration of rainfall (Jiang et al., 2020; Auler and Smart, 2003), so the influence of the relative change in the rock–soil ratio and soil layer thickness is different over a short time, but the difference is not obvious on the interannual scale.

4.4. Hydrological responses of subsurface leakage to rainfall events

The relationship between the daily rainfall and the daily leakage (Fig. 9) shows that the relationship between daily leakage and daily rainfall in the rainy season is the same as that in the whole year. However, in rainfall events, there are obvious differences between the rainy season and dry season, and the leakage of epikarst with cracks is obviously high. Water can flow rapidly along the rock and redistribute in the epikarst zone because of the cracks present (Fu et al., 2015; Zhang et al., 2013a). Many studies of natural watersheds show that rainfall intensity has a significant influence on the peak value and duration of spring discharge, but the effect of the epikarst zone on the peak discharge is small (Ding et al., 2020). Moreover, if the total amount of discontinuous rainfall is more than 6 mm and the rainfall intensity is more than 0.8 mm/h, a spring will cause the corresponding occurrence unless there is a recent rainstorm to wet the soil (Winston and Criss, 2004). The flow will also be affected by antecedent rainfall (Fu et al., 2015; Liu et al., 2015; Wang et al., 2020a,b). From the relationship between rainfall and leakage in the dry season, it can be seen that when the rainfall is less than 15 mm/h, the leakage of the four rock–soil structures does not increase significantly, which is mainly due to the soil drought, and the rainwater is stored in the soil or rock pores, resulting in the reduction of leakage. However, when the rainfall is 0.8 mm/h and 9.2 mm/h, the leakage of structures with rock exposure rate of 80% is 4.06 mm/h and 1.59 mm/h, respectively, which is higher than that of structures with rock exposure rate of 50%, that is caused by the rapid infiltration of rainwater along the crack and the delay effect under a certain rainfall intensity.

4.5. Implications

Karst areas are usually characterized by high biodiversity and great heterogeneity in ecological patterns and hydrological processes (Clements et al., 2006). The topsoil in karst areas is thin, and epikarst zones with fractures are the key to vegetation transpiration and water storage and transportation (Zhang et al, 2013b). Continuous monitoring on an hourly scale in this study reveals the impact of the rock–soil structure on surface and subsurface hydrological processes, especially the hydrological response characteristics after different rainfall intensities. On the one hand, the research results provide a reference basis for using a model to estimate surface water evaporation in different regions. Owing to evaporation from rock may be an important part of surface evaporation, evaporation from rock should be considered in sprinkler irrigation measures in rock-exposed areas, rational planning of irrigation facilities and water conservation. On the other hand, for areas with cracks and thin soil, the groundwater hydrological response is fast, thus it should be considered in the design and construction of small water cellar in the high-level depressions in karst areas according to local

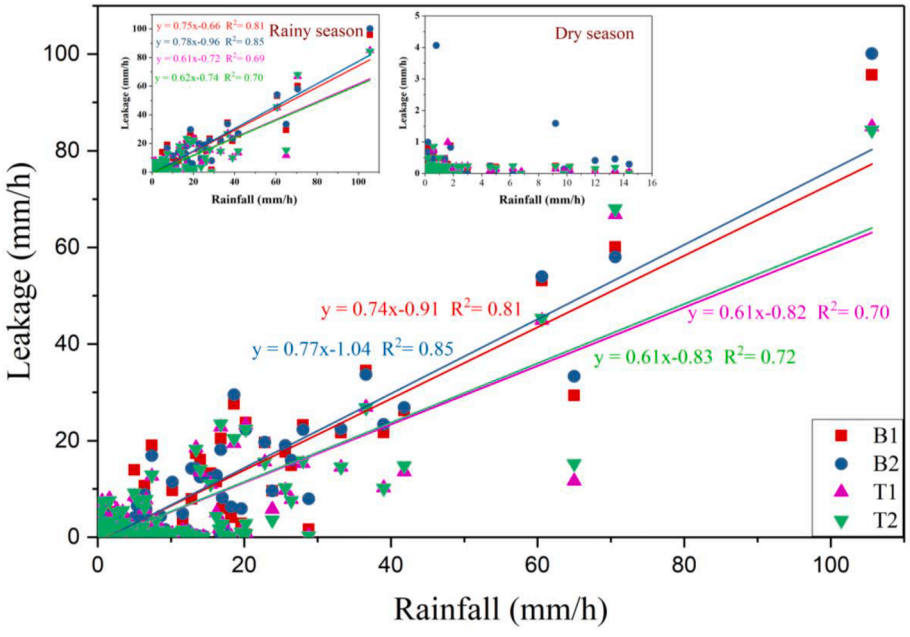

Fig. 9. The relationship between rainfall and leakage.

conditions, and irrigate sporadic cultivated land in the dry season. Reasonable drainage measures such as ditches and trenches should be established in low-lying areas to reduce waterlogging disasters in rainy season. The research results can provide not only a scientific reference for water use and management, such as ecological restoration, drought prevention and drainage in karst areas with different rock exposure rates, soil layer thicknesses and rainfall intensities, but also valuable information for the later study of the hydrological processes between rock and soil–plant–atmosphere continuum (SPAC) systems in karst areas. However, bedrock can also affect surface vegetation (Praeg et al., 2017; Jiang et al., 2020), and the hydrological processes influenced by rock–soil–plant–atmosphere interactions are worthy of further exploration.

In addition, this study was based on the simulated experimental and has obtained some understanding, but there are still some limitations. For example, the top fine soil will migrate/penetrate into the dolomitic particles in subsequent rain events, and when there is a variation in partial pressure of CO_2 values, the dissolution of carbonates in an evaporation prevailing environment tends to dissolve the carbonates and precipitates in the pore spaces. What is the influence of these processes on the permeability and porosity of the simulated experimental, which needs to be further explored. Moreover, a variety of research methods should be combined to conduct comparative research and verification of natural catchments and simulated experimental in the future.

5. Conclusions

Evaporation is mainly affected by net radiation and relative humidity in the dry season, while in the rainy season, it is mainly affected by temperature, wind speed and net radiation. When the rock exposure rate at the lysimeter increased from 50% to 80%, the surface evaporation was reduced by approximately 8%, while the difference in evaporation between the two structures with different soil thicknesses was only 2%. The evaporation of rock moisture may be a part of surface evaporation, which affects the surface evaporation after different rainfall intensities, while the evaporation from surfaces without exposed rocks has no significant difference after different rainfall intensities. Cracks and soil thickness have little effect on the leakage coefficient, but the leakage coefficient with or without cracks is quite different. The leakage of the epikarst zone is significantly affected by rainfall intensity, but the rock–soil structure will also affect the leakage and the time to reach the peak flow and is affected by the antecedent rainfall. These findings can provide a scientific reference for water use and management practices such as ecological restoration, drought prevention and drainage in karst areas, and valuable information for the later study of the hydrological processes between rock and soil–plant–atmosphere continuum (SPAC) systems in karst areas.

CRediT authorship contribution statement

Jia Chen: Conceptualization, Methodology, Software, Investigation, Writing – original draft. **Weijun Luo:** Validation, Formal analysis, Data curation, Supervision, Writing – review & editing. **Guangneng Zeng:** Validation, Formal analysis, Data curation, Supervision, Writing – review & editing. **Yanwei Wang:** Data curation, Writing – review & editing. **Yina Lyu:** Data curation, Writing – review & editing. **Xianli Cai:** Data curation, Writing – review & editing. **Lin Zhang:** Resources, Data curation. **Anyun Cheng:** Resources, Data curation, Writing – review & editing. **Xinbao Zhang:** Data curation, Supervision, Writing – review & editing. **Shijie Wang:** Data curation, Supervision, Writing – review & editing, Resources.

Declaration of Competing Interest

The authors declare that they have no known competing financial interests or personal relationships that could have appeared to influence the work reported in this paper.

Acknowledgments

This work was jointly supported by the Strategic Priority Research Program of the Chinese Academy of Sciences (XDB40020200), the National Natural Science Foundation of China (41673121 41663015), Guizhou Science and Technology Cooperation Basic Project([2020] 1Y188). We sincerely thank the anonymous reviewers for their valuable comments and suggestions.

References

Andreo, Bartolomé, 2012. Introductory editorial: advances in karst hydrogeology. Environ. Earth Sci. 65 (8), 2219–2220.
Auler, A.S., Smart, P.L., 2003. The influence of bedrock-derived acidity in the development of surface and underground karst: evidence from the Precambrian carbonates of semi-arid northeastern Brazil. Earth Surf. Proc. Landf. 28 (2), 157–168.
Bakalowicz, M., 2005. Karst groundwater: a challenge for new resources. Hydrogeol. J. 13 (1), 148–160.
Butscher, C., Huggenberger, P., 2009. Modeling the temporal variability of karst groundwater vulnerability, with implications for climate change. Environ. Sci. Technol. 43 (6), 1665–1669.
Chen, H.S., Yang, J., Fu, W., et al., 2020. Characteristics of slope runoff and sediment yield on karst hill-slope with different land-use types in northwest Guangxi. Transactions of the Chinese Society of Agricultural Engineering. 28 (16), 121–126.
Clements, R., Sodhi, N.S., Schilthuizen, M., Ng, P.K.L., 2006. Limestone karsts of southeast Asia: imperiled arks of biodiversity. Bioscience. 56, 733–742.
Coleman, G., Decoursey, D.G., 1976. Sensitivity and Model Variance Analysis Applied to Some Evaporation and Evapotranspiration Models. Water Resour Res. 12 (5), 873–879.
Ding, H., Zhang, X., Chu, X., Wu, Q., 2020. Simulation of groundwater dynamic response to hydrological factors in karst aquifer system. Journal of Hydrology. 587, 124995.
Ferreira, L., Marotta, G. S., Madden, E. H., Horbe, A. M. C., Santos, R. V., Costa, J. M. N., 2021. Vertical displacement caused by hydrological influence in the Amazon Basin. J Geophys Res-Sol Ea. 126, e2020JB020691.
Ford, D.C., Williams, P.M., 2007. Karst Hydrogeology and Geomorphology. John Wiley & Sons Ltd, England.
Fu, W., Chen, H.S., Wang, K.L., 2007. Variability in soil moisture under five land use types in Karst hillslope territory. Chinese Journal of Eco-Agriculture. 15 (5), 59–62.
Fu, Z.Y., Chen, H.S., Zhang, W., Xu, Q.X., Wang, S., Wang, K.L., 2015. Subsurface Flow in a Soil-Mantled Subtropical Dolomite Karst Slope: A Field Rainfall Simulation Study. Geomorphology. 250, 1–14.
Goldscheider, N., Chen, Z., Auler, A.S., Bakalowicz, M., Broda, S., Drew, D., Hartmann, J., Jiang, G., Moosdorf, N., Stevanovic, Z., Veni, G., 2020. Global distribution of carbonate rocks and karst water resources. Hydrogeology Journal 28 (5), 1661–1677.
Gong, L.B., Xu, C.Y., Chen, D.L., Halldin, S., Chen, Y.Q.D., 2006. Sensitivity of the Penman-Monteith reference evapotranspiration to key climatic variables in the Changjiang (Yangtze River) basin. J Hydrol. 329 (3–4), 620–629.
Hamilton, J., Ford, D., 2002. Karst geomorphology and hydrogeology of the Bear Rock Formation: a remarkable dolostone and gypsum megabreccia in the continuous permafrost zone of Northwest Territories. Canada. Carbonates Evaporites. 17 (2), 114–115.
Hao, Y., Zhao, J., Li, H., Cao, B., Li, Z., et al., 2012. Karst hydrological processes and grey systemmodel. J. Am. Water Resour. Assoc. 48 (4), 656–666.
Hartmann, A., Mudarra, M., Andreo, B., Marín, A., Wagener, T., Lange, J., 2014. Modeling spatiotemporal impacts of hydroclimatic extremes on groundwater recharge at a Mediterranean karst aquifer. Water Resour Res. 50 (8), 6507–6521.
Hu, Y., Liu, Z., Zhao, M., Zeng, Q., Zeng, C., Chen, B.o., Chen, C., He, H., Cai, X., Ou, Y.i., Chen, J., 2018. Using deuterium excess precipitation and runoff data to determine evaporation and transpiration A case study from the Shawan Test Site, Puding, Guizhou. China. Geochimica et Cosmochimica Acta. 242, 21–33.
Jiang, Z., Liu, H., Wang, H., Peng, J., Meersmans, J., Green, S.M., Quine, T.A., Wu, X., Song, Z., 2020. Bedrock geochemistry influences vegetation growth by regulating the regolith water holding capacity. Nature communications. 11 (1).
Jones, I.C., Banner, J.L., Humphrey, J.D., 2000. Estimating recharge in a tropical karst aquifer. Water Resour. Res. 36 (5), 1289–1299.
Lenters, J.D., Kratz, T.K., Bowser, C.J., 2005. Effects of climate variability on lake evaporation: Results from a long-term energy budget study of Sparkling Lake, northern Wisconsin (USA). J Hydrol. 308 (1–4), 168–195.
Liu, C., Yang, J., Nie, Y.P., Chen, H.S., Fu, Z.Y., 2015. Hydrochemical responses of stromflow to extreme rainfall during dry season in a typical karst catchment of northwest Guangxi province China. Earth and Environment. 43 (4), 386–394.
Luo, M.M., Xiao, T.Y., Chen, Z.H., et al., 2014. Geological structure characteristics of several karst water systems in the Xiangxi River Karst Basin. Hydrogeology and Engineering. Geology. 41, 13–19.
Massei, N., Mahler, B.J., Bakalowicz, M., Fournier, M., Dupont, J.P., 2007. Quantitative interpretation of specific conductance frequency distributions in karst. Groundwater 45 (3), 288–293.

Nie, Y.P., Chen, H.S., Wang, K.L., Yang, J., 2012. Water source utilization by woody plants growing on dolomite outcrops and nearby soils during dry seasons in karst region of Southwest China. J Hydrol. 420, 264–274.
Nouri, M., Homaee, M., Bannayan, M., 2017. Quantitative Trend, Sensitivity and Contribution Analyses of Reference Evapotranspiration in some Arid Environments under Climate Change. Water Resour Manag. 31 (7), 2207–2224.
Peng, T., Wang, S.J., 2012. Effects of land use, land cover and rainfall regimes on the surface runoff and soil loss on karst slopes in southwest China. Catena. 90, 53–62.
Poesen, J., Lavee, H., 1994. Rock fragments in top soils: significance and processes. Caneta 23 (1-2), 1–28.
Poulain, A., Watlet, A., Kaufmann, O., Van Camp, M., Jourde, H., Mazzilli, N., Rochez, G., Deleu, R., Quinif, Y., Hallet, V., 2018. Assessment of groundwater recharge processes through karst vadose zone by cave percolation monitoring. Hydrol. Process. 32 (13), 2069–2083.
Praeg, N., Wagner, A.O., Illmer, P., 2017. Plant species, temperature, and bedrock affect net methane flux out of grassland and forest soils. Plant Soil. 410 (1-2), 193–206.
Seneviratne, S.I., Corti, T., Davin, E.L., Hirschi, M., Jaeger, E.B., Lehner, I., Orlowsky, B., Teuling, A.J., 2010. Investigating soil moisture–climate interactions in a changing climate: a review. Earth Sci. Rev. 99 (3-4), 125–161.
Rempea, D.M., Dietrich, W.E., 2018. Direct observations of rock moisture, a hidden component of the hydrologic cycle. PNAS. 115 (11), 2664–2669.
Shen, Y., Wang, D., Chen, Q., Tang, Y., Chen, F., 2019. Large heterogeneity of water and nutrient supply derived from runoff of nearby rock outcrops in karst ecosystems in SW China. Catena. 172, 125–131.
Sohrt, J., Ries, F., Sauter, M., Lange, J., 2014. Significance of preferentialflow at the rock soil interface in a semi-arid karst environment. Catena 123, 1–10.
Stevanovic, Z., 2018. Global distribution and use ofwater from karst aquifers. In: Parise, M., Gabrovsek, F., Kaufmann, G., Ravbar, N. (Eds.), Advances in Karst Research: The- ory. London, Special Publications, Fieldwork and Applications, Geological Society, pp. 217–236.
Wang, F.a., Chen, H., Lian, J., Fu, Z., Nie, Y., 2020a. Hydrological response of karst stream to precipitation variation recognized through the quantitative separation of runoff components. Science of the Total Environment. 748, 142483.
Wang, S., Fu, Z., Chen, H., Nie, Y., Xu, Q., 2020b. Mechanisms of surface and subsur- face runoff generation in subtropical soilepikarst systems: implications of rainfall simulation experiments on karst slope. J. Hydrol. 580, 124370.
Wang, S.J., Zhang, X.B., Bai, X.Y., 2015. An outline of karst geomordhology zoning in the karst areas of southern China. Mountain research. 33 (6), 641–648.
Wilcox, B.P., Wood, M.K., Tromble, J.M., 1988. Factors influencing infiltrability of semiarid mountain slopes. J. Range Manag. 41 (3), 197–206.
Winston, W.E., Criss, R.E., 2004. Dynamic hydrologic and geochemical response in a perennial karst spring. Water Resour. Res. 40, W05106.
Wu, Z.Y., Xue, L., Zhang, X.S., et al., 2021. Spatial Variability of Soil Moisture under Typical Vegetation Types on Karst Dolomite Slope in Dry Season. Forest Research 34 (4), 74–83.
Zeng, Q., Liu, Z., Chen, B.o., Hu, Y., Zeng, S., Zeng, C., Yang, R., He, H., Zhu, H., Cai, X., Chen, J., Ou, Y.i., 2017. Carbonate weathering-related carbon sink fluxes under different land uses: A case study from the Shawan Simulation Test Site, Puding, Southwest China. Chemical Geology 474, 58–71.
Zeppel, M., Macinnis-Ng, C.M.O., Ford, C.R., Eamus, D., 2008. The response of sap flow to pulses of rain in a temperate Australian woodland. Plant Soil 305 (1–2), 121–130.
Zhang, R., Xu, X., Liu, M., Zhang, Y., Xu, C., Yi, R., Luo, W., 2018. Comparing evapotranspiration characteristics and environmental controls for three agroforestry ecosystems in a subtropical humid karst area. J. Hydrol. 563, 1042–1050.
Zhang, Z., Chen, X.i., Chen, X., Shi, P., 2013a. Quantifying Time Lag of Epikarst Spring Hydrograph Response to Rainfall Using Correlation and Spectral Analyses. Hydrogeol. J. 21 (7), 1619–1631.
Zhang, Z.-C., Chen, X.i., Shi, P., Ou, G.-X., 2013b. Study of canopy transpiration based on a distributed hydrology model in a small karst watershed of southwest China. Carbonates and Evaporites. 28 (1-2), 111–117.
Zhao, M., Zeng, C., Liu, Z., Wang, S., 2010. Effect of different land use/land cover on karst hydrogeochemistry: a paired catchment study of Chenqi and Dengzhanhe, Puding, Guizhou, SW China. Journal of Hydrology. 388 (1-2), 121–130.
Zhao, Z., Shen, Y., Wang, Q., Jiang, R., 2020. The temporal stability of soil moisture spatial pattern and its influencing factors in rocky environments. Catena 187, 104418.
Zhao, Z., Shen, Y., Shan, Z., Yu, Y., Zhao, G., 2018. Infiltration Patterns and Ecological Function of Outcrop Runoff in Epikarst Areas of Southern China. Vadose Zone J. 17 (1), 170197.
Zheng, H., Yu, G.R., Wang, Q.F., Zhu, X.J., He, H.L., Wang, Y.F., Zhang, J.H., Li, Y.N., Zhao, L., Zhao, F.H., Shi, P.L., Wang, H.M., Yan, J.H., Zhang, Y.Y., 2016. Spatial variation in annual actual evapotranspiration of terrestrial ecosystems in China: Results from eddy covariance measurements.J. Geogr. Sci. 26 (10), 1391–1411.
Zou, S.Z., Zhang, W.H., Liang, X.P., Luo, W.Q., Liang, B., 2005. Quantitative calculation of regulating coefficient for epikarst zone—Case study of Zhaojiawan, Luota, West of Hunan. Hydrogeology & Engineering Geology. 4, 37–42.